Laser heating of particles in dusty plasmas

Matthias Wolter and André Melzer
Institut für Physik, Ernst-Moritz-Arndt-Universität Greifswald, 17487 Greifswald, Germany
(Received 30 November 2004; published 30 March 2005)

Experiments on the heating and melting of two-dimensional finite dust crystals are performed using random laser excitation of the dust particles by a rapidly moving laser beam. The achievable dust temperatures scale with the square of the laser power. The heating process is described for different dust clusters under various plasma and cluster conditions. A single-particle model is developed to explain the observed behavior of the cluster under the random laser excitation. Good quantitative agreement is found when the radiation pressure is made responsible for the particle excitation by the laser. The dynamical properties of the system during heating are analyzed and the dominant modes are identified. From this, it is demonstrated that the heating process is of a nearly equilibrium nature in contrast to previous melting experiments. Finally, the melting of the dust cluster by laser heating is studied. From these experiments, a precise determination of the critical coupling parameter for the solid-fluid transition was possible. It is measured as $\Gamma = 270-480$ for an $N=18$ cluster.

DOI: 10.1103/PhysRevE.71.036414 PACS number(s): 52.27.Lw, 45.50.−j, 52.25.Kn

I. INTRODUCTION

In a weakly ionized dusty plasma, suspended micrometer-sized dust particles usually are negatively charged with charges of the order of $Z \approx 10^4$ elementary charges per particle. The strong Coulomb interaction between dust particles leads to the formation of dust Coulomb crystals and liquids [1,2]. In typical laboratory experiments on strongly coupled dusty plasmas, monodisperse micrometer-sized particles are trapped in a parallel-plate rf discharge [2–5]. In the sheath above the lower electrode, the weight of the particles is balanced by the electric field force acting on them. There, the particles are confined to a flat cloud that is of large horizontal extent and limited in the vertical direction due to this force balance.

One of the most interesting problems in dusty plasmas is the thermodynamic properties of strongly coupled Coulomb systems. Strong coupling is defined using the Coulomb coupling parameter

$$\Gamma = \frac{Z^2 e^2}{4\pi\varepsilon_0 b_{\mathrm{WS}} k T_{\mathrm{d}}} \tag{1}$$

that describes the Coulomb interaction of neighboring particles in units of their thermal energy kT_{d}. In two-dimensional (2D) systems which will be discussed here, the particle separation is characterized by the Wigner-Seitz radius $b_{\mathrm{WS}} = 1/\sqrt{\pi n_{\mathrm{d}}}$, where n_{d} is the 2D density of the dust particles. The system is said to be strongly coupled when the coupling parameter exceeds unity. When the coupling parameter exceeds a critical threshold value of $\Gamma_c = 130 \pm 5$ for pure Coulomb interaction in 2D [6], the particles arrange in a regularly ordered crystalline arrangement, a Wigner or plasma crystal.

The shielding of the dust particles by the surrounding plasma is described by an additional parameter, the screening strength

$$\kappa = b_{\mathrm{WS}}/\lambda_D, \tag{2}$$

which is the Wigner-Seitz distance in units of the Debye length λ_D. The phase diagram of three-dimensional (3D) strongly coupled systems in the Γ-κ plane is well investigated [7,8]. It is found that the critical threshold for crystallization Γ_c increases nearly exponentially with κ. For 2D systems, the phase diagram is much more difficult to derive, since according to the Kosterlitz-Thouless-Halperin-Nelson-Young (KTHNY) theory of 2D melting [9], the phase transition is in two steps, both of which are second-order transitions. Only a few values of the melting line in 2D systems are reported in the literature [10,11].

Experimentally, phase transitions have been observed in two-layer and multilayer systems with reducing the gas pressure [12–14] or in monolayer systems with increasing particle density [15]. Those experiments exploit the nonequilibrium environment of the sheath where the particles are trapped. There the dust particles are heated due to instabilities arising from the nonequilibrium situation in the sheath [10].

In the experiments presented here, we mimic an equilibrium heating process for the dust particles by a random laser excitation of the individual dust particles. This is achieved by randomly pointing the laser beam to different particles in the plasma crystal using a galvanometer scanner with a rapid scanning procedure. The heating and melting of plasma crystals using this laser heating mechanism is investigated here.

Lasers are a widely applicable tool in dusty plasmas for the manipulation of individual particles. They have been applied, e.g., for the excitation of waves and Mach cones [16–22] or for the measurement of attractive forces in plasma crystals [23,24] as well as for the excitation of shear flows in fluid particle arrangements [25,26].

Our experiments on laser heating and melting have been performed in finite 2D systems, so-called Coulomb clusters with $N=10$ to about $N=200$ particles. 2D Coulomb clusters are characterized by their total energy [27,28],

$$E = \frac{1}{2} m \omega_0^2 \sum_{i=1}^{N} r_i^2 + \frac{Z^2 e^2}{4\pi\epsilon_0} \sum_{i>j}^{N} \frac{\exp(-r_{ij}/\lambda_D)}{r_{ij}}, \quad (3)$$

where the first term is the potential energy of the *horizontal* confinement with the horizontal resonance frequency ω_0 and the second term is the Coulomb energy of all particles. Here, m denotes the mass of the dust particles, $r_i = |\vec{r}_i|$ is the radial coordinate of particle i, and $r_{ij} = |\vec{r}_i - \vec{r}_j|$ is the distance between particles i and j. After normalizing the energy to $E_0 = [Z^2 e^2 m \omega_0^2/(8\pi\epsilon_0)]^{1/3}$ and the radial coordinate to $r_0 = [2Z^2 e^2/(4\pi\epsilon_0 m \omega_0^2)]^{1/3}$, the total energy can be written as

$$E = \sum_{i=1}^{N} r_i^2 + \sum_{i>j}^{N} \frac{\exp(-r_{ij}\kappa')}{r_{ij}}, \quad (4)$$

where $\kappa' = r_0/\lambda_D$. The screening strength κ' is generally applied in the description of 2D clusters and uses the normalized distance r_0. In contrast, the above-mentioned screening strength κ is related to the Wigner-Seitz radius b_{WS}. These two definitions of the relevant distance differ by a factor of 4 in our experiments, namely $r_0 \approx 4 b_{WS}$. Thus the screening strengths also behave as $\kappa' \approx 4\kappa$. In this paper, we follow the definition of κ with the Wigner-Seitz distance.

In this article, we first introduce the laser excitation and heating method, which is then applied to different clusters where the equilibrium nature of the heating processes is investigated and where the heating is applied to clusters under different plasma conditions. Thereafter, a model is developed that describes the laser heating and the dependence on the plasma and crystal properties. Then, the dynamical properties during heating and, finally, the melting of the dust clusters are described.

II. EXPERIMENTAL METHOD

The experiments are performed in an argon rf plasma discharge at 13.56 MHz between two large horizontal electrodes at gas pressures between 5 and 10 Pa. The upper electrode is the grounded cap of the vacuum vessel. The lower electrode is powered at 2–8 W at a maximum rf voltage of 15 V_{pp}. A metal plate of 70 mm diameter with a spherical trough of 3 mm depth was used and placed in the center of the lower electrode to create the horizontal parabolic confinement potential. The schematic experimental setup is shown in Fig. 1.

The dust particles in our experiments are monodisperse spherical plastic particles (melamine formaldehyde) with a diameter of $2a = 9.55$ μm and of mass $m = 6.90 \times 10^{-13}$ kg. In some cases, particles with $2a = 12.25$ μm and $m = 1.46 \times 10^{-12}$ kg have been used. The particles are injected from a dust dropper above the lower electrode. The dust dropper is a small container with a 300 μm hole in the bottom. By weakly shaking the dust dropper from outside, a few particles at a time fall through the hole into the experimental area. The particles are trapped in a monolayer in the sheath above the lower electrode, where the electric field force balances gravity. The horizontal confinement is due to the shallow trough.

The dust particles are illuminated by a laser diode (50 mW at 685 nm). The particles are viewed by a CCD camera from the side to verify that the particles are trapped in a monolayer. The main diagnostic tool is the top view camera, a CMOS camera with a maximum frame rate of 500 frames per second (fps). In our experiment, the camera is operated at 50 fps for about 25 s, which amounts to typically 1200 frames in total. An interference filter at 685 nm is used in front of the high-speed camera to block the light from the Nd:YAG manipulation laser.

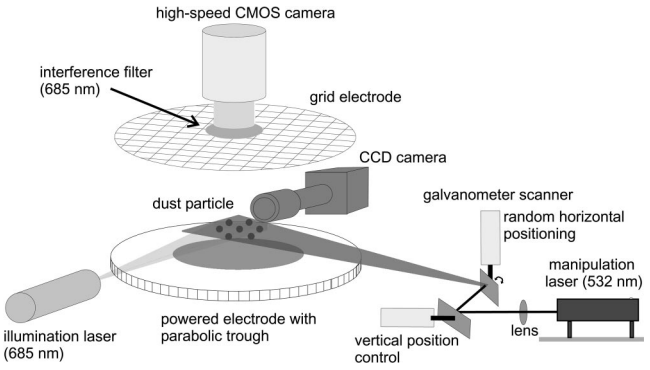

FIG. 1. Scheme of the experimental setup. The particles find their equilibrium position above the powered electrode. The particles can be manipulated by the focused beam of the manipulation laser. The beam is steered in the discharge by the two-axis galvanometer scanner.

For particle manipulation, a Nd:YAG laser at 532 nm with a maximum output power of 200 mW is applied. This laser is focused onto the particles in the dust cloud. The manipulation laser beam is controlled by a galvanometer scanning system. The scanner consist of two mirrors, one for the horizontal deflection and one for the vertical deflection of the incoming laser beam. With this galvanometer scanner, the position and motion of the laser beam are controlled. Thus, it is possible to manipulate a single particle, a group of particles, or the entire cluster.

To mimic a random heating of the dust cluster, the following procedure was applied. Vertically, the laser beam is kept at a fixed position at the height of the dust cloud. Horizontally, the laser beam is swept randomly across the entire clus-

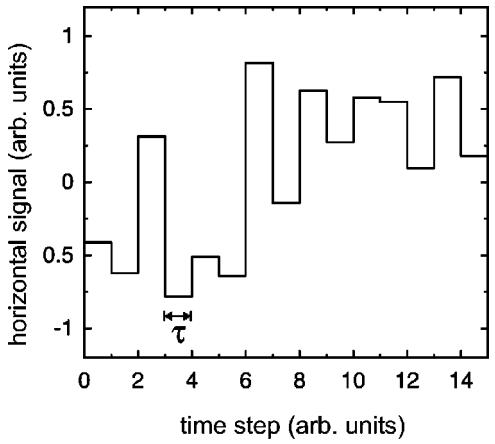

FIG. 2. A short sequence of the signal to the horizontal galvanometer scanner. The horizontal angular deflection of the laser beam is proportional to the signal applied to the scanner.

ter to randomly push the various particles of the cluster (see Fig. 2). Each angular position is held for a certain time step τ of the order of 10 ms. So, the force exerted by the beam is active for this time step τ if a particle is hit by the laser beam (by chance, the beam might also point to a position in the cluster where no particles are present). The maximum angular excursions during the scan are chosen in such a way that the entire cluster is covered. In our experiments, the "heating" power of the manipulation laser beam can be varied between $P=0$ mW and 200 mW.

III. RESULTS AND DISCUSSION

A. Heating

With the first experiment, the possibility of heating single particles or the entire plasma crystal with the manipulation laser is explored. For this purpose, the laser beam was swept randomly as described above and the manipulation laser power was increased from 0 mW to 200 mW. For each laser power setting, the particle trajectories have been recorded. In this experiment, the rf power was 8 W and the argon gas pressure was 5 Pa. The investigated crystal consists of 18 dust particles with a diameter of 9.55 μm.

The trajectories of the particles at different manipulation laser powers are shown in Fig. 3. It is seen that the motion of the dust particles increases with increasing laser power. Obviously, kinetic energy is transferred to the particles by the laser beam. To quantify this behavior, the corresponding particle temperature T_d was measured. The notion of temperature is related to the random kinetic energy for a two-dimensional system as

$$\sum_{i=1}^{N} \frac{m}{2}\langle v_i^2\rangle = NkT_d, \tag{5}$$

where v_i is the velocity of the ith particle, k is Boltzmann's constant, and the brackets indicate the temporal average. When using the term "particle temperature" in the following, we refer to the mean kinetic energy averaged over all particles and frames. The measured particle temperatures during the laser heating are shown in Fig. 4.

From this, it is seen that the particle temperature grows stronger than linear with manipulation laser power. The increase of particle temperature can be described by a square law. Such a dependence is characteristic for all our measurements. Furthermore, different temperatures for the x and y direction are observed (we define the y direction as the direction of the laser beam and the x direction as perpendicular in the monolayer cluster plane). Obviously, the laser stimulates the particles preferably in the direction of the beam: The particles get a higher energy, and thus a higher temperature, in the y direction. Nevertheless, due to particle-particle repulsion in the cluster, the energy in the beam direction gets randomized and thus also the perpendicular direction is heated. Since the x temperature also scales like a square law, a constant fraction of the energy in the beam direction is transferred to the perpendicular.

The solid lines in Fig. 4 represent a quadratic fit to the data, with

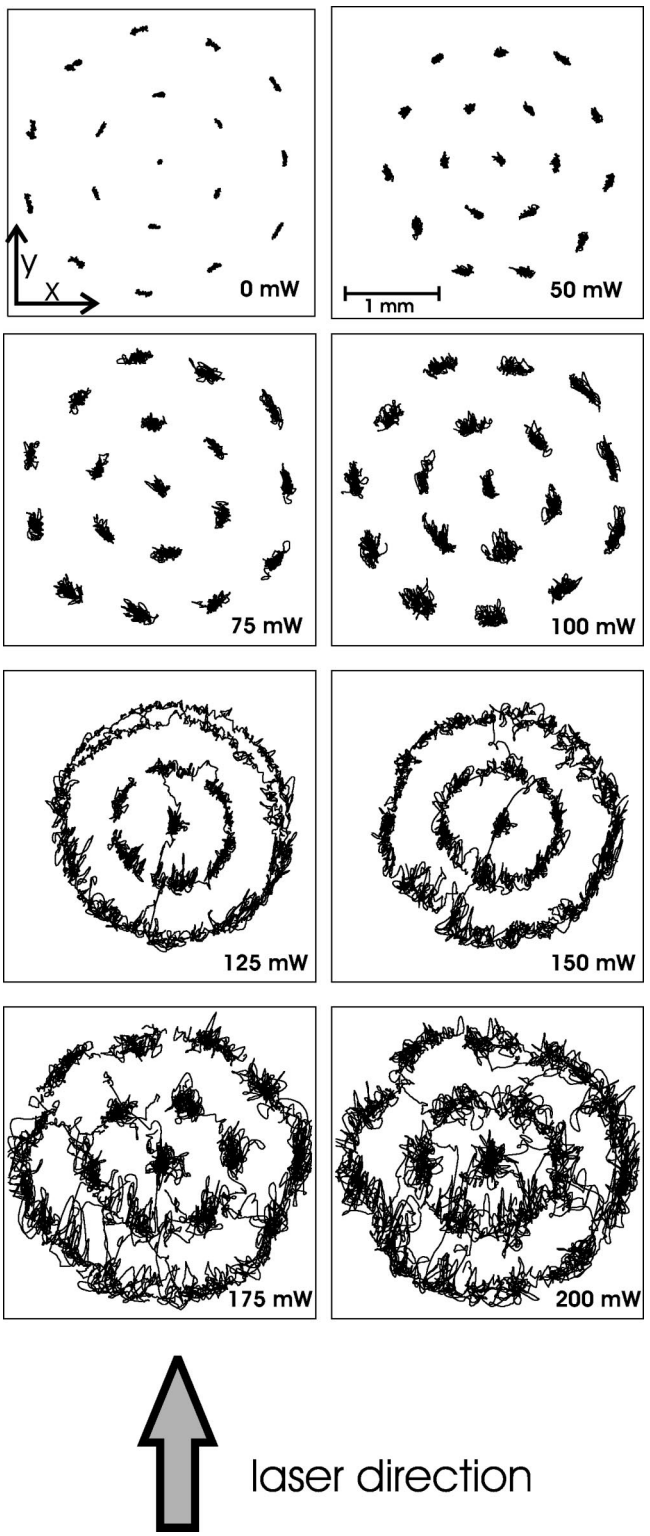

FIG. 3. Dust particle trajectories over 50 s for increasing manipulation laser beam intensity between 0 mW and 200 mW. The manipulation laser beam travels along the y direction.

$$T_d = CP^2,$$

where P is the laser power. The constant C is obtained from the fit as $C_y=93\ \mathrm{eV/W^2}$ for the y temperature and C_x

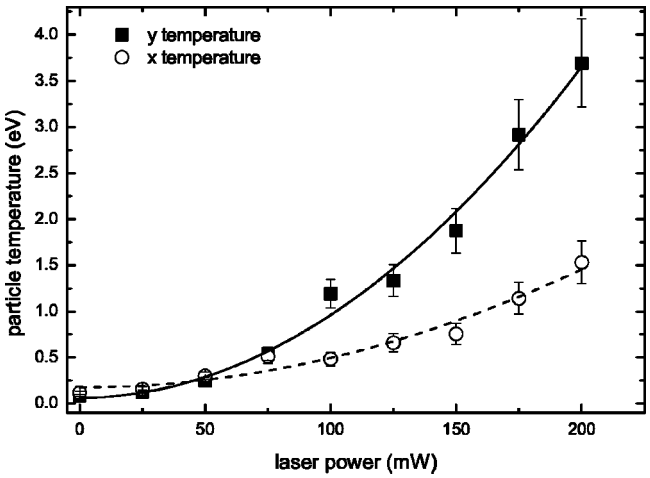

FIG. 4. Average particle temperatures for the x and y direction with increasing manipulation laser power. The solid lines represent a quadratic fit to the results of the measurement.

$=43\ \mathrm{eV/W^2}$ for the x temperature. The relative error of our temperature measurements is around 15%.

One open question is whether the notion of particle temperature is justified here under the conditions of a finite particle ensemble and a limited time series. This is studied from the velocity distribution of the particles. The velocity distribution in the y direction of all particles and time steps is shown in Fig. 5 for the cluster at 0 mW and 200 mW, respectively.

With laser "off," the distribution function is very narrow and very close to a Maxwellian. For a laser power of 200 mW, the distribution is much broader and deviations from the Maxwellian distribution are observed: for velocities between 0 and +1500 μm/s, the distribution is below the expected Maxwellian, whereas for higher velocities the measured distribution is larger than expected. Thus, the laser beam preferentially excites large velocities in the direction of the beam.

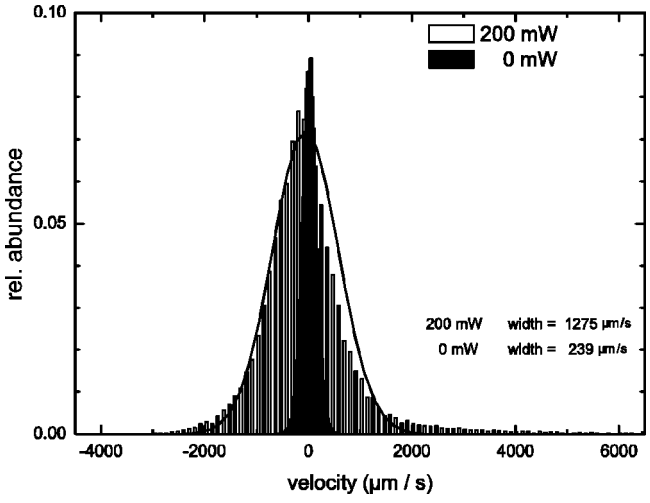

FIG. 5. The velocity distribution function of the $N=18$ particles. In the case of 0 mW manipulation laser power, a very narrow velocity distribution is found. At 200 mW, deviations from a Maxwellian distribution are seen.

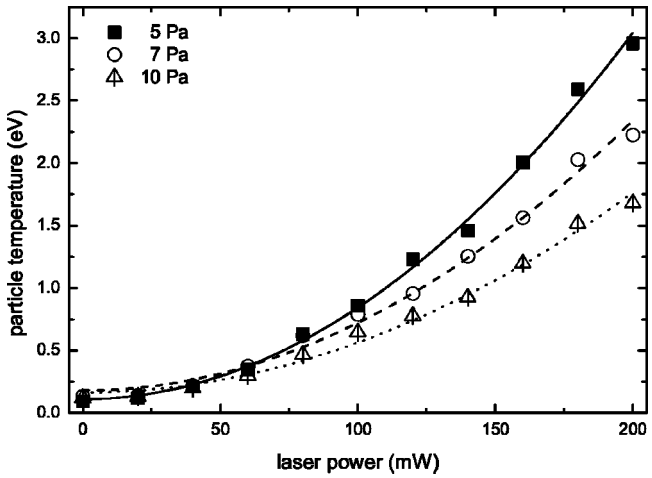

FIG. 6. Particle temperature as a function of laser power for different gas pressures. Here, only the y component of the temperature is shown.

The dust temperature can also be deduced from the full width at half maximum of a Maxwellian fit to the measured data. Here, we find a particle temperature of 0.13 eV at 0 mW and for 200 mW the particle temperature is 3.69 eV. Compared to the temperature derived from Eq. (5), there is very good agreement for both cases ($T_d=0.09$ eV at 0 mW and $T_d=3.70$ eV at 200 mW). The differences are readily explained by the deviations from the exact Maxwellian distribution. Nevertheless, the distribution functions are close enough to Maxwellian to justify the use of "particle temperature."

In the undisturbed state at 0 mW, we find a mean particle temperature (x and y direction) of 0.11 eV ($\approx$1250 K). This result agrees with the results of Nunomura *et al.* [19,29] and Melzer [30]. Nunomura reported temperatures in extended 2D plasma crystals between 440 K and 530 K. Melzer found temperatures between 370 K and 1300 K for various different finite dust clusters.

B. Parameter variation

In the next steps, the parameter of the cluster and the discharge plasma have been varied. First, the results of the change of gas pressure between 5 and 10 Pa are shown in Fig. 6.

With increasing gas pressure, the particle temperature decreases for a given laser power. Increased gas pressure results in more effective friction of the particles with the neutral gas. Thus, the heated particles are more efficiently cooled and the observed temperature is decreased. The achieved temperatures scale approximately as the inverse of the gas pressure.

Second, the number of particles in the cluster was modified at constant discharge parameters (rf power 8 W, gas pressure 5 Pa, particle diameter 9.55 μm). With increasing particle number, the dust cluster grows in size. The scan amplitude was set in such a way that the laser beam completely covers the largest cluster used in our experiments with $N=218$ particles. When using fewer dust particles, the

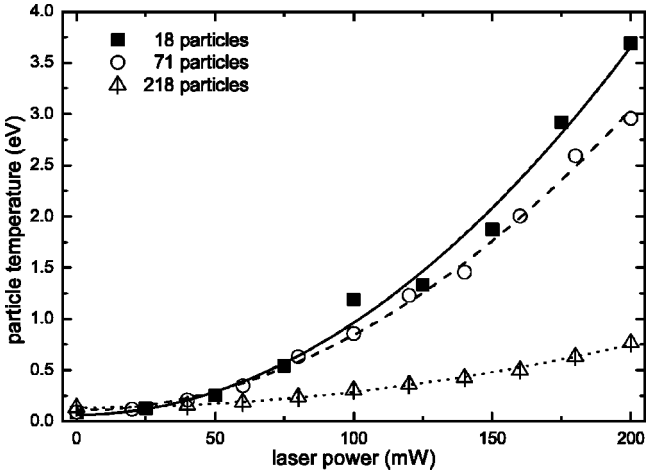

FIG. 7. Dust temperature as a function of laser power for different cluster sizes. With increasing number of particles, the dust temperature decreases.

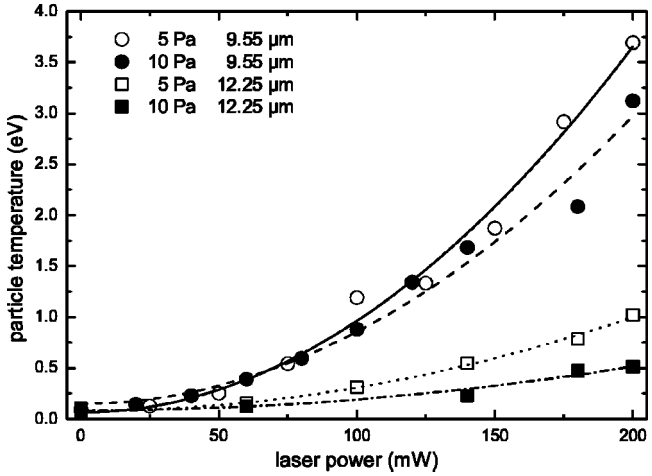

FIG. 8. Heating of the particles for different particle sizes and discharge pressures.

scan amplitude was unchanged to ensure the same number of laser excitation pulses per angular range. The observed particle temperature depends on the number of particles in the cluster, as shown in Fig. 7.

With the fewest number of particles ($N=18$), the temperature is about 3.68 eV at 200 mW whereas with 71 particles we find a temperature of 2.96 eV and with the most particles ($N=218$) in the cluster the temperature decreases to 0.75 eV. Since the laser energy per angle is kept constant and the diameter (i.e., the angular width) of the dust cloud D scales as $D \propto \sqrt{N}$, the total laser energy transferred to the cluster is proportional to $\sqrt{N}$. Hence, we would expect that the energy per particle and thus the temperature decreases as $T_d \propto 1/\sqrt{N}$. A decrease of dust temperature with particle number is observed, but the proposed scaling is only roughly fulfilled.

In the third part of parameter variation, the particle temperature is studied for different particle sizes. The same experimental conditions as before are applied and particles with a diameter of 9.55 μm and 12.25 μm are used. The results of this experiment are shown in Fig. 8.

There is a strong difference in particle temperature with different size. For the smaller particles (9.55 μm), a high particle temperature (depending on the pressure) between 3 and 4 eV is found. For the larger particles, the particle temperature decreases dramatically to 1 and 0.5 eV at 5 and 10 Pa, respectively. A functional behavior is difficult to estimate from these data.

In this and the previous section, we have collected the following properties for heating of dust clusters by a laser beam. We have demonstrated that heating of the cluster by random excitation of the particles results in an increased particle temperature. The achieved dust temperature scales with the square of the laser power and is inversely proportional to the gas pressure. The dust temperature decreases with particle number in the cluster and with particle size where a clear functional behavior is difficult to find.

C. Model

In the following, we attempt to model the observed heating behavior of the dust cluster. Due to the random excitation, a single particle is illuminated by the laser beam for the time τ (see Fig. 2). During that time, the particle is accelerated by the laser-particle interaction. When the laser is swept to a different position and the particle is no longer illuminated, the particle motion is damped by the presence of the neutral gas. Thus, the equation of motion of a single particle is given by

$$m\ddot{y} + m\beta\dot{y} = F_l \quad \text{for } 0 < t < \tau, \tag{6}$$

$$m\ddot{y} + m\beta\dot{y} = 0 \quad \text{for } t > \tau. \tag{7}$$

Here, β is the Epstein coefficient [31] due to friction with the neutral gas and is given by

$$\beta = \frac{8}{\pi} \frac{p}{\rho a v_{\text{th,n}}},$$

where p is the gas pressure, ρ is the mass density of the dust particle, and $v_{\text{th,n}}$ is the thermal velocity in the neutral gas. Moreover, y is an excursion of the particle from its equilibrium position. F_l is the force exerted by the laser on the particle and is assumed to be constant with position. We will discuss the possible forces below.

The solution of the equation of motion is (for $0 < t < \tau$)

$$y = \frac{F_l}{m\beta^2}(\beta t + e^{-\beta t} - 1). \tag{8}$$

In our experiments, τ is of the order of 10 ms and the damping constant β is of the order of 1 s^{-1}. Thus, $\beta t \ll 1$ and the above solution can be written as

$$y(t) = \frac{F_l t^2}{2m} \text{ and } v_y(t) = \frac{F_l}{m} t \text{ for } 0 < t < \tau. \tag{9}$$

The excitation phase is just a constantly accelerated motion; damping effects are not important during that time span. When the laser is moved to the next angular position, the particle motion is damped. Thus, the velocity at the end of the acceleration process decays exponentially like

$$v_y(t) = \frac{F_1 \tau}{m} \exp[-\beta(t-\tau)] \text{ for } t > \tau. \quad (10)$$

The mean kinetic energy requires the knowledge of $\langle v_y(t)^2 \rangle$. For the entire heating and damping process, this is given by

$$\langle v_y(t)^2 \rangle = \frac{1}{T}\left[\int_0^\tau \frac{F_1^2}{m^2} t^2 dt + \int_\tau^T \frac{F_1^2 \tau^2}{m^2} \exp[-2\beta(t-\tau)] dt \right]. \quad (11)$$

The time T is the time over which the process is averaged. This period is the time after which the particle is again hit by the laser beam and the heating is started anew. This time is given by the number of different angular positions and the time step τ for each angular position. Since the angular variation is done randomly, this time can only be given as the mean time between two laser hits. From our experiments, we estimate that value to be $T \approx 0.5$ s.

Under the justified assumption that $\tau \ll T$, we find

$$\langle v_y(t)^2 \rangle = \frac{F_1^2 \tau^2}{2m^2 \beta T}(1 - e^{-2\beta T}) \quad (12)$$

and thus the particle temperature as

$$kT_\mathrm{d} = \frac{m}{2}\langle v_y(t)^2 \rangle = \frac{F_1^2 \tau^2}{4m\beta T}(1 - e^{-2\beta T}). \quad (13)$$

Now the question remains which is the possible force exerted by the laser F_l. In the literature, two possible forces are discussed, namely the radiation pressure F_rad and the photophoretic force F_ph. The radiation pressure is due to the momentum exerted by the laser photons hitting the dust particle. This force is proportional to the laser power P and is given by [32]

$$F_\mathrm{rad} = \gamma \frac{P}{A_f c} \pi a^2, \quad (14)$$

where A_f is the area onto which the laser is focused and $\gamma = 1, \ldots, 2$ is the reflection coefficient that describes how the photons are reflected from the dust particle.

The photophoretic force is due to heating of one side of the dust particle surface by the laser. Neutral gas atoms reflected from the hotter side get a larger momentum than those from the colder. Thus a force directed away from the hot side (and thus in the direction of the laser beam) is exerted on the dust. The photophoretic force is also proportional to the laser power as [33]

$$F_\mathrm{ph} = \frac{\pi a^3 p}{6 \varkappa T_n} \frac{P}{A_f}, \quad (15)$$

where p is the gas pressure and $\varkappa$ is the thermal conductivity of the dust particle. The above expression is valid under the assumption that the particle is small compared to the mean free path in the gas and that the front side of the particle is heated. The exact calculation of the force is quite difficult and requires the calculation of the laser field inside the particle [34]. The force can even be opposite to the laser beam.

Both forces are proportional to the laser power and thus the dust temperature according to Eq. (13) is proportional to the square of the laser power as observed in the experiment. Since the friction coefficient β scales with pressure, the dust temperature scales as $T_d \propto 1/p$ when the laser force is given by the radiation pressure. The photophoretic force, however, is itself proportional to the pressure. Thus the temperature would scale as $T_d \propto p$. Since the experiments suggest an inverse scaling with pressure, the radiation pressure is supported.

The scaling with cluster size is already discussed in the previous section. In the notation of the equation, this means that the time until a particle is again hit by the laser beam will increase as $T \propto \sqrt{N}$.

Finally, the scaling with particle size: Here, the model proposes a scaling with $T_d \propto a^2$ for the radiation pressure (note that $m \propto a^3$ and $\beta \propto 1/a$ and $F_\mathrm{rad} \propto a^2$). For the photophoretic force, we find an even stronger scaling as $T_d \propto a^4$. Both forces predict that larger particles will be heated more strongly, which, however, is not seen in the experiment.

The quantitative agreement of our simplified model with the experimental findings is quite remarkable. Using the experimental values for the situation in Fig. 4, we find for the radiation pressure force

$$C = \frac{T_d}{P^2} = 160 \text{ eV/W}^2$$

when the following values are used: $\beta = 10$ 1/s, $T = 0.5$ s, $\tau = 10$ ms, $\gamma = 1$ (absorbed photons), and $A_\mathrm{f} = \pi R^2$ with $R = 200$ μm. This value compares reasonably with the experimental value of $C = 93$ eV/W^2. The photophoretic force would result in a heating constant that is larger by a factor 2000, which is drastically different from the experiment. However, as mentioned above, the photophoretic force is strongly dependent on the exact optical properties of the particles and would require the determination of the light field distribution within the particle. This is beyond the scope of this paper.

The model treats the excitation as a single-particle effect. The fact that more than one particle can be heated by the laser beam at the same time is not included. Furthermore, the randomization due to interaction with the other particles is not covered. Moreover, also the Coulomb interaction with the other particles in the cluster is neglected here.

Nevertheless, the proposed model captures the main observations of the experiment, especially when the laser force is given by the radiation pressure. The photophoretic force does not seem to be very appropriate for the description of the laser heating.

D. Mode analysis

In the first set of experiments, we have investigated the global characteristics of the dust cluster in dependence of various plasma and cluster parameters. Here, we are interested in the dynamical properties of the cluster. One of the main questions is which modes are preferably excited during the laser heating process.

The dynamical properties of a finite dust cluster are described in terms of their eigen or normal modes. The normal modes of a 2D cluster are calculated from the dynamical matrix [28]

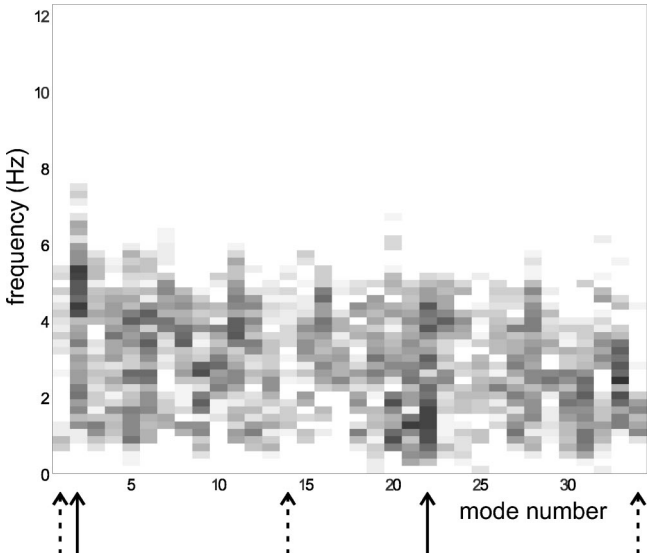

FIG. 9. Measured mode spectrum of the $N=18$ cluster. The spectral power density is shown in gray scale. Modes 1, 14, and 34 show a very low spectral power density, whereas modes 2 and 22 have very high power densities.

$$E_{\alpha\beta,ij} = \frac{\partial^2 E}{\partial r_{\alpha,i} \partial r_{\beta,j}}, \tag{16}$$

where E is the total energy according to Eq. (4) and $r_{\alpha,\beta}$ denote either the x or y coordinate and i,j is the particle number. The normal mode frequencies ω_ℓ of the 2N modes are the eigenvalues of the dynamical matrix (in units of $\omega_0/\sqrt{2}$) and its eigenvectors describe the mode oscillation patterns [28].

Experimentally, the eigenmodes are derived from the thermal motion of the dust particles [30]. There, first the particle velocities are projected onto the oscillation pattern of mode ℓ by $f_\ell(t)=\Sigma_{i=1}^{N}\vec{v}_i(t)\cdot\vec{e}_{i,\ell}$. Here, $\vec{e}_{i,\ell}$ denotes the eigenvector of the ith particle for mode number ℓ. The function $f_\ell(t)$ is a time series that contains the contribution of the thermal particle motion for mode ℓ. Then, the spectral power density $S_\ell(\omega)$ of $f_\ell(t)$ is calculated. This gives the energy stored in this mode in the frequency domain. This procedure is repeated for all $2N$ eigenmodes of the cluster. For details of this method, see Ref. [30].

The mode spectrum of the already discussed $N=18$ cluster is shown in Fig. 9 as a gray-scale plot. Dark regions correspond to large power densities. In previous experiments without laser heating [30], the power density in the modes was found to be equally distributed among the modes. Here, with laser heating present, it is seen that some modes acquire high spectral power densities whereas others get only low power densities. The modes 2 and 22 are very intense modes with a high spectral power density (marked by the solid arrow). Weak modes with minimum power densities are modes 1, 14, and 35 (dashed arrow).

This visual impression is substantiated by calculating the energy stored in the different modes or, equivalently, the temperature corresponding to this mode. The effective temperature of each cluster mode is readily extracted from the normal mode spectra. Therefore, we make use of the relation

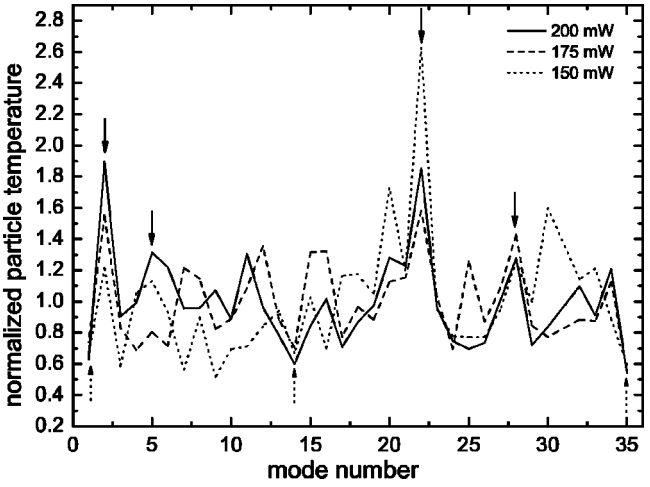

FIG. 10. Normalized particle temperatures for manipulation laser powers of 150 mW, 175 mW, and 200 mW. When comparing with Fig. 9, the low power-density modes and high power-density modes manifest in low and high mode temperatures, respectively.

$$\int_0^\infty S_\ell(\omega)d\omega = \langle v_\ell^2 \rangle \tag{17}$$

that yields the mean-square particle velocity of mode number ℓ. Consequently, we can assign a temperature for mode ℓ as

$$\frac{1}{2}kT_{\mathrm{mode},\ell} = \frac{m}{2}\langle v_\ell^2 \rangle. \tag{18}$$

A single effective temperature of the entire cluster T_{mode} can be obtained from the mean of the mode temperatures, i.e.,

$$kT_{\mathrm{mode}} = \frac{1}{N}\sum_{\ell=1}^{2N}\frac{1}{2}m\langle v_\ell^2 \rangle = \frac{1}{2N}\sum_{\ell=1}^{2N} kT_{\mathrm{mode},\ell}. \tag{19}$$

Now, Fig. 10 shows the mode temperatures $T_{\mathrm{mode},\ell}$ for the different mode numbers. The temperatures have been normalized to the mean mode temperature T_{mode} here. This has been done to compare the situation at different laser powers, namely 150, 175, and 200 mW. As expected from the mode spectrum, the modes with the highest temperatures are mode numbers 2 and 22, which have temperatures that are about a factor of 1.8 above the mean temperature of $T_{\mathrm{mode}}=2.82$ eV. The modes 1, 14, and 35 have the lowest temperatures of about $0.6T_{\mathrm{mode}}$. This quantifies the observation from the mode spectra.

When repeating this analysis for laser beam powers of 150 and 175 mW, a similar behavior as for the 200 mW case is observed. The corresponding mode temperatures for these cases are also shown in Fig. 10. Comparing the situation for all three laser powers, one finds local maxima of the particle temperature for *all* laser powers at mode numbers 2 and 22 and to a lesser extent for modes 5 and 28. Pronounced minima for *all* laser powers are observed for modes 1, 14, and 35.

The oscillation pattern of these pronounced modes is shown in Fig. 11. Modes 2 and 5 are modes with high activ-

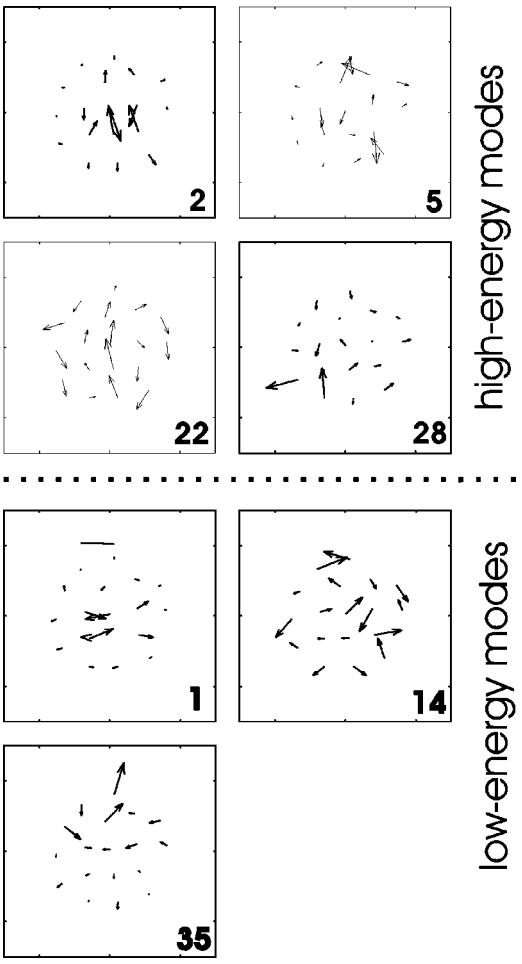

FIG. 11. Oscillation pattern of the pronounced high-energy modes 2, 5, 22, and 28, as well as of the low-energy modes 1, 14, and 35.

ity in the cluster center. The main particle motion is in the y direction, i.e., the direction of the laser beam. Mode 28 is somewhat difficult to characterize. Mode activities are at the boundary, also with some preference in the y direction. The most pronounced peak belongs to mode number 22 that describes a vortex-antivortex pair that is oriented along the laser beam. From this it is obvious that the laser beam preferably excites modes that favor the particle motion in the direction of the beam.

The low-energy modes do not show such a clear structure: Mode 1 has high central activity, for mode 35 most activity is at the boundary, and for mode 14 overall particle motion is indicated. However, for all these low-energy modes it is seen that the particle oscillations are preferably in the x direction, perpendicular to the beam. This explains why these modes are least likely excited by the laser beam.

One important point should be noted here. Although a few modes are more heated than others, energy is transferred to all modes. The difference in the excitation is not that large. In contrast, in two-layer systems which are heated and melted due to the nonreciprocal attraction between the two layers, the heating is due to an unstable oscillation that manifests in a dominant nonequilibrium excitation of all modes at a single frequency [35]. In comparison, the laser heating comes close to an equilibrium heating of the cluster and thus the thermodynamic properties of the system can be studied in equilibrium.

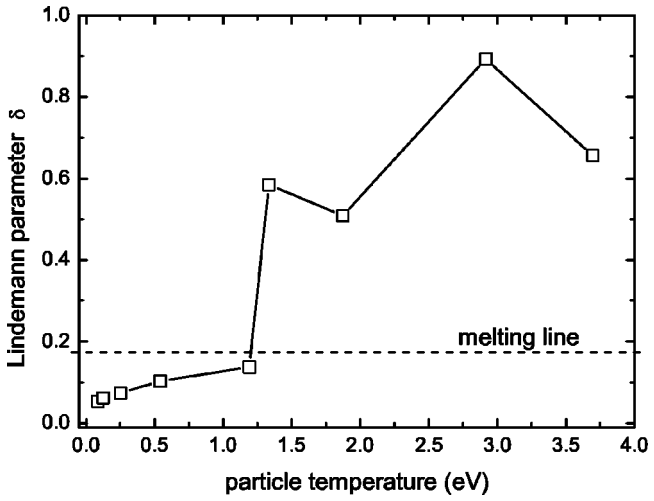

FIG. 12. Lindemann parameter as a function of the particle temperature. The Lindemann parameter exceeds the threshold of 0.18 for particle temperatures larger than 1.19 eV. This temperature corresponds to a laser power of 100 mW.

E. Melting

After the heating experiments and the dynamical analysis of the cluster heating, the question follows whether it is possible to create a phase transition or melting of the dust cluster.

The trajectories of the $N=18$ cluster during heating are already shown in Fig. 3. At a manipulation laser power of 125 mW and more, very excited particle motions are observed that indicate a phase transition from solid to the liquid state. This visual estimation can be substantiated from the calculation of the order or Lindemann parameter δ. In a 2D system, the Lindemann parameter is defined as the root-mean-square deviation of the particle from its equilibrium position relative to the nearest-neighbor particles. Then, the order parameter can be written as

$$\delta^2 = \frac{1}{Na^2}\left\langle \sum_{i=1}^{N} \frac{1}{N_b} \sum_{j=1}^{N_b} |\vec{u}_i(t) - \vec{u}_j(t)|^2 \right\rangle, \qquad (20)$$

where N_b is the number of neighboring particles to particle i, and $\vec{u}_i$ is the relative displacement of particle i from its equilibrium position. Bedanov *et al.* [36] state that for 2D systems, the melting transition occurs when the Lindemann parameter exceeds the critical value $\delta_c = 0.18$.

For the $N=18$ cluster, the Lindemann parameter together with the measured temperature is shown in Fig. 12. The parameter δ exceeds the threshold at temperatures between 1.19 eV and 1.33 eV (corresponding to laser powers between 100 and 125 mW). For higher laser powers (temperatures) the order parameter is decisively above the threshold. Just at this critical temperature (laser power), a lot of particle motion in the trajectories (Fig. 3) with exchange of equilibrium positions is observed.

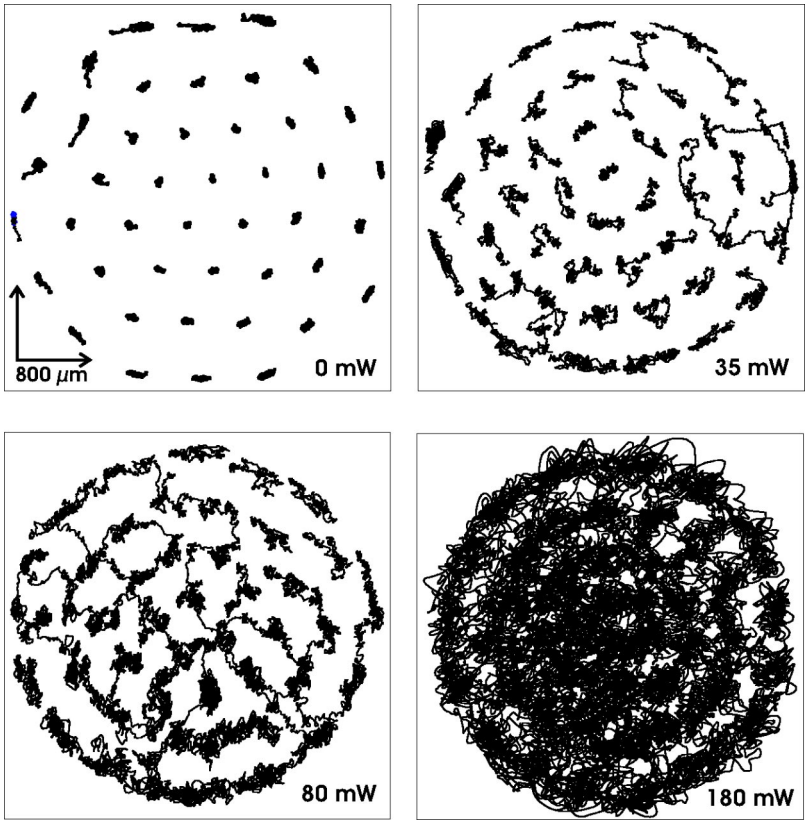

FIG. 13. Dust particle trajectories over 50 s for increasing manipulation laser beam intensity between 0 mW and 200 mW with higher laser density.

From the analysis of the mode spectra during the melting transition, the strength of the horizontal confinement ω_0 and the screening strength κ is derived. This is achieved by fitting the measured mode frequencies to the theoretical frequencies that depend on these two parameters. This method is illustrated in more detail in [30]. Good agreement of the measured frequencies with the theoretical mode frequencies is obtained for screening strengths in the range of $\kappa = b_{WS}/\lambda_D = 0.25, \ldots, 1$ and $\omega_0/2\pi \approx 1$ Hz, which is in good agreement with earlier observations [30].

After that, the particle charge is obtained from the absolute size of the system. In the solid state (at the temperature of 1.19 eV), it is found to be as $Z = 11\,200 \pm 1000$, where the error range is due to the uncertainty in κ; for the fluid state (at the temperature of 1.33 eV), we obtain $Z = 8800 \pm 700$.

We are thus now able to determine the critical value of Γ for the transition from the fluid to the solid state from our laser heating. For the solid state, the coupling parameter is found to be $\Gamma_{solid} = 480 \pm 80$, and in the fluid state it is found to be $\Gamma_{fluid} = 270 \pm 43$. Thus the phase transition of the dust cluster should occur at a Γ between 270 and 480. The critical values of Γ_c for the fluid-solid transition in 2D systems found from simulations [10,11] are $\Gamma_c = 132$ for $\kappa = 0$ and $\Gamma_c = 151$ for $\kappa = 1$.

Our lower and upper boundaries for the fluid-solid transition are in reasonable agreement with the theoretical expectations. One should note that in the experiment, the dust density is not homogeneous, which would lead to a position-dependent critical Γ_c. Moreover, the simulated values correspond to infinite 2D systems. From 3D Coulomb clusters, it is known that the critical Γ_c increases with decreasing particle number of finite systems [37]. For 2D clusters, Totsuji [38] gives a rough estimate of $100 < \Gamma_c e^{-\kappa} < 2000$ since radial and azimuthal melting occurs at very different temperatures [28].

Since, as discussed above, the laser heating is nearly an equilibrium process, the observed critical Γ describes the thermodynamic properties of the dust cluster. These laser melting experiments allow us to determine this transition with unprecedented accuracy.

Finally, in a refined experiment, we improved the focus of the manipulation laser beam. Figure 13 shows the trajectories for the then increased laser power density and Fig. 14 shows the measured temperature and corresponding Lindemann pa-

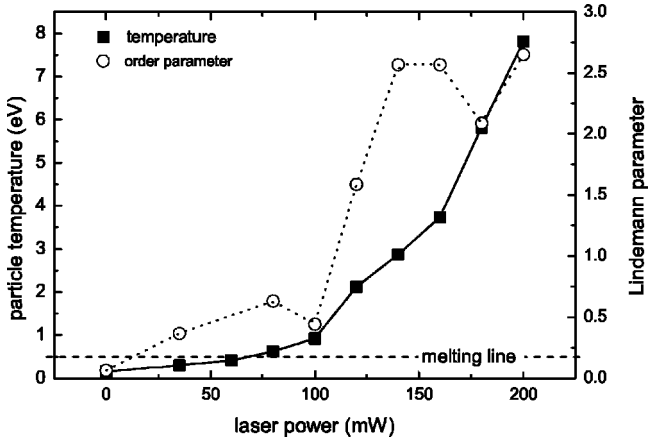

FIG. 14. Particle temperature and Lindemann parameter as a function of laser power. With the improved focus, the phase transitions of the cluster are observed at a lower manipulation laser beam power (35 mW).

rameter. The cluster investigated here consists of $N=44$ particles.

With the refined focus, the particle temperature is increased by a factor of 3 under the same plasma conditions. Consequently, a phase transition into the fluid state is already observed for the first laser power setting (35 mW). There the coupling parameter is found to be around $\Gamma \approx 800$. The solid state at 0 mW has $\Gamma = 3000 \pm 500$. Thus, the critical Γ for this $N=44$ particle cluster is larger than that of the $N=18$ cluster and is still in the range given by Totsuji [38].

IV. SUMMARY

We have presented experiments for heating and melting processes under different conditions in a dusty plasma crystal. The dust temperature increases with the square of the laser power. We have demonstrated that the particle size, the number of particles, and the gas pressure play a decisive role in the heating and melting of dusty plasma crystals. The achievable dust temperature is inversely proportional to the gas pressure and decreases with increasing particle number and particle size.

A model was presented that captures the main properties of the heating and that accurately models the dependence on the plasma and crystal properties. This model was based on the analysis of the equation of motion of a single particle in a cluster under random heating. Good agreement between the model and the experiments was found when the particles were assumed to be excited through radiation pressure. The photophoretic force gives only poor agreement.

The dynamical properties have been derived from a mode analysis during heating. The mode analysis reveals that predominantly those modes are heated that require particle motions in the direction of the beam, whereas modes with perpendicular particle motions are decisively less heated. Nevertheless, the deviation from equipartition between the modes is not that large. This finding and the analysis of the velocity distribution function suggest that the heating process can be characterized as nearly equilibrium.

Finally, laser-induced melting of the cluster has been achieved. More importantly, we were able to measure the critical value for fluid-solid phase transitions in our clusters. It was found to be between $\Gamma = 270$ and 480 for the $N=18$ cluster and around $\Gamma = 1000$ for the $N=44$ cluster. This is in agreement with simulations of 2D cluster melting. Despite this uncertainty, this is still a quite precise measurement of the critical Coulomb coupling parameter in dusty plasmas.

We have demonstrated that laser excitation techniques are a perfect tool for the investigation of heating in dusty plasmas. The laser manipulation system developed for these investigations will be applied in experiments on parabolic flights in 2005 and 2006, when the application potential of the laser manipulation will be tested under microgravity conditions.

ACKNOWLEDGMENTS

We gratefully acknowledge financial support from DLR under Contract No. 50 WM 0338.

[1] J. H. Chu and L. I, Phys. Rev. Lett. **72**, 4009 (1994).
[2] H. Thomas, G. E. Morfill, V. Demmel, J. Goree, B. Feuerbacher, and D. Möhlmann, Phys. Rev. Lett. **73**, 652 (1994).
[3] J. H. Chu, J.-B. Du and L. I, J. Phys. D **27**, 296 (1994).
[4] Y. Hayashi and K. Tachibana, Jpn. J. Appl. Phys., Part 2 **33**, L804 (1994).
[5] A. Melzer, T. Trottenberg, and A. Piel, Phys. Lett. A **191**, 301 (1994).
[6] S. Ichimaru, Rev. Mod. Phys. **54**, 1017 (1982).
[7] M. O. Robbins, K. Kremer, and G. S. Grest, J. Chem. Phys. **88**, 3286 (1988).
[8] S. Hamaguchi, R. Farouki, and D. H. E. Dubin, Phys. Rev. E **56**, 4671 (1997).
[9] K. Strandburg, Rev. Mod. Phys. **60**, 161 (1988).
[10] V. A. Schweigert, I. V. Schweigert, A. Melzer, A. Homann, and A. Piel, Phys. Rev. Lett. **80**, 5345 (1998).
[11] I. V. Schweigert, V. A. Schweigert, and F. Peeters, Phys. Rev. Lett. **82**, 5293 (1999).
[12] A. Melzer, A. Homann, and A. Piel, Phys. Rev. E **53**, 2757 (1996).
[13] H. Thomas and G. E. Morfill, Nature (London) **379**, 806 (1996).
[14] R. A. Quinn, C. Cui, J. Goree, J. B. Pieper, H. Thomas, and G. E. Morfill, Phys. Rev. E **53**, R2049 (1996).
[15] A. Ivlev, U. Konopka, G. Morfill, and G. Joyce, Phys. Rev. E **68**, 026405 (2003).
[16] A. Homann, A. Melzer, S. Peters, R. Madani, and A. Piel, Phys. Rev. E **56**, 7138 (1997).
[17] A. Homann, A. Melzer, R. Madani, and A. Piel, Phys. Lett. A **242**, 173 (1998).
[18] A. Melzer, S. Nunomura, D. Samsonov, and J. Goree, Phys. Rev. E **62**, 4162 (2000).
[19] S. Nunomura, D. Samsonov, and J. Goree, Phys. Rev. Lett. **84**, 5141 (2000).
[20] S. Nunomura, J. Goree, S. Hu, X. Wang, and A. Bhattacharjee, Phys. Rev. E **65**, 066402 (2002).
[21] V. Nosenko, J. Goree, Z. W. Ma, and A. Piel, Phys. Rev. Lett. **88**, 135001 (2002).
[22] V. Nosenko, S. Nunomura, and J. Goree, Phys. Rev. Lett. **88**, 215002 (2002).
[23] K. Takahashi, T. Oishi, K. Shimomai, Y. Hayashi, and S. Nishino, Phys. Rev. E **58**, 7805 (1998).
[24] A. Melzer, V. Schweigert, and A. Piel, Phys. Rev. Lett. **83**, 3194 (1999).
[25] H.-Y. Chu, Y.-K. Chiu, C.-L. Chan, and L. I, Phys. Rev. Lett. **90**, 075004 (2003).
[26] V. Nosenko and J. Goree, Phys. Rev. Lett. **93**, 155004 (2004).
[27] V. M. Bedanov and F. Peeters, Phys. Rev. B **49**, 2667 (1994).
[28] V. A. Schweigert and F. Peeters, Phys. Rev. B **51**, 7700 (1995).

[29] S. Nunomura, J. Goree, S. Hu, X. Wang, A. Bhattacharjee, and K. Avinash, Phys. Rev. Lett. **89**, 035001 (2002).
[30] A. Melzer, Phys. Rev. E **67**, 016411 (2003).
[31] P. S. Epstein, Phys. Rev. **23**, 710 (1924).
[32] A. Ashkin, Phys. Rev. Lett. **24**, 156 (1970).
[33] A. M. Ignatov and S. G. Amiranashvili, Phys. Rev. E **63**, 017402 (2001).
[34] Y. lin Xu, B. A. S. Gustafson, F. Giovane, J. Blum, and S. Tehranian, Phys. Rev. E **60**, 2347 (1999).
[35] R. Ichiki, Y. Ivanov, M. Wolter, Y. Kawai, and A. Melzer, Phys. Rev. E **70**, 066404 (2004).
[36] V. M. Bedanov, G. Gadiyak, and Y. E. Lozovik, Phys. Lett. **109**, 289 (1985).
[37] J. P. Schiffer, Phys. Rev. Lett. **88**, 205003 (2002).
[38] H. Totsuji, Phys. Plasmas **8**, 1856 (2001).